RESEARCH ARTICLE

Experimental study on a -86 °C cascade refrigeration unit with environmental-friendly refrigerants R290-R170

Zhan Liu[1,2] · Kaifeng Yuan[1] · Yunzhi Ling[1] · Haihui Tan[3] · Shuo Yang[2]

Abstract

Ultralow-temperature refrigeration faces significant issues linked to the security of the cold chain for the production, storage, transportation, and distribution of COVID-19 vaccines. The use of environmentally friendly refrigerants in cascade refrigeration systems (CRS) to provide low-temperature range is motivated by the high demand for ultralow-temperature refrigeration units. In the current study, a CRS is built to generate a low temperature of -86 °C for the storage of COVID-19 vaccines. In the CRS, the natural refrigerant combination R290-R170 is used as high-temperature and low-temperature fluids. The pull-down performance of the -86 °C freezer is explored experimentally, and the stable operating performance is determined at two different dry bulb and wet bulb temperatures. Various status monitors are set up to analyze the CRS's operation features, and several temperature monitors are put in the freezer to analyze temperature variations. The power consumption of the CRS is examined and evaluated. Finally, several key findings are summarized. The current work is the first to involve experimental measurements on -86 °C temperature generated by a CRS, which can substantially enhance experiment data in ultralow-temperature refrigeration and contribute to a more in-depth understanding of the operation performance of a -86 °C ultralow-temperature freezer.

Keywords COVID-19 vaccines storage · Cascade refrigerant system · -86 °C ultralow-temperature · Environmental-friendly refrigerants · Experimental test

Introduction

In response to the COVID-19 pandemic, ultralow-temperature refrigeration is urgently required throughout the development, storage, transportation, and distribution of Sars-CoV-2 vaccines, and the number of ultralow-temperature freezers has expanded dramatically around the world. Some pharmaceutical companies, such as Pfizer-BioNTech, have claimed that their vaccines must be stored at temperatures ranging from -60 °C to -80 °C. This means that the COVID-19 vaccinations have stringent criteria for low-temperature storage freezers. According to American Society of Heating, Refrigerating, and Air-Conditioning Engineers (ASHRAE) (2014), ultralow-temperature refrigeration can be described as the storage of equipment at or below -50 °C and can also extend to the evaporation temperature of -100 °C (Mota-Babiloni et al. 2020).

CRS appears to be a better option for producing ultralow temperature. In general, the CRS operates with two or more serially disposed cycles and has a freezing temperature of < -60 °C. According to certain researchers (Mumanachit et al. 2012, Pan et al. 2020, Mateu-Royo et al. 2021), two-stage CRS is more efficient at low-temperature refrigeration, particularly in commercial supermarkets and industrial sectors. Chlorofluorocarbons (CFCs) refrigerants were mostly phased out due to their high Ozone Depletion Potential (ODP) and Global Warming Potential (GWP), particularly in developed countries. Hydrofluorocarbons

✉ Zhan Liu
liuzhanzkd@cumt.edu.cn

1 State Key Laboratory of Intelligent Construction and Healthy Operation and Maintenance of Deep Underground Engineering, School of Mechanics and Civil Engineering, China University of Mining and Technology, Xuzhou 221116, China

2 Department of Energy Sciences, Faculty of Engineering, Lund University, 22100 Lund, Sweden

3 School of Mechanical and Electrical Engineering, University of Electronic Science and Technology of China, Zhongshan Institute, Zhongshan 528400, China

(HFCs), a CFC substitute refrigerant, emit greenhouse gases. A transition to natural refrigerants appears to be unavoidable in the near future. Countries all over the world are focusing on natural refrigerants to help with global warming. Carbon dioxide R744 and N_2O (R744A) are the most effective natural refrigerants. The fundamental disadvantage of R744 and R744A as low-temperature refrigerants is that both have a high operating pressure. Despite this, many researchers continue to believe that both are potential refrigerants for low-temperature refrigeration due to their zero ODP and low GWP.

Researchers conducted numerous theoretical analyses and experimental tests by employing R744 as a low-temperature refrigerant (LTR) in CRS. Lee et al. (2006) carried out a thermodynamic analysis on a R744-ammonia (R717) CRS in order to increase the COP and prevent exergy destruction in refrigeration system by regulating the condensing temperature of the cascade heat exchanger (CHE). It was discovered that the ideal COP increases with low-temperature cycle (LTC) evaporating temperature and decreases with high-temperature cycle (HTC) condensing temperature. To optimize the R744-R717 CRS's operating parameter, Getu and Bansal (2008) performed a thorough thermodynamic analysis. To estimate the ideal COP and refrigerant mass flow ratio between HTC and LTC, a multilinear regression analysis was used with the consideration of subcooling, superheating, evaporating and condensing temperatures, and CHE temperature difference. Bingming et al. (2009) experimentally evaluated the performance of a R744-R717 CRS with a twin-screw compressor. They discovered that the R744-R717 CRS had the maximum COP when the evaporation temperature was less than -40 °C. Dopazo and Fernández-Seara (2011) investigated the performance of a R744-R717 CRS with a refrigeration capacity of 9 kW and an evaporation temperature of -50 °C in an experimental study. The highest variation is roughly 2.4% when compared to optimum condensing temperature computed using different calculation correlations. Llopis et al. (2015) investigated the operation of four direct two-stage systems and a CRS with R744 as LTR. They discovered that direct CO_2 transcritical two-stage systems are not suitable for usage in warm nations, however the CRS using R744 as LTR has good application prospects for commercial refrigeration in hot climates. Eini et al. (2016) performed a multi-objective optimization on a CRS from perspectives of economics, exergy, and the environment. The results revealed that R744-R717 and R744-R290 CRSs have nearly same economic and exergy efficiency, whereas R744-R717 CRS has intrinsic safety. Cabello et al. (2017) compared the performance of a CRS using R744 as LTR and R134a and R152a as high-temperature refrigerants (HTRs). The results revealed that the operation performance of the R134a-R744 CRS is comparable to that of the R152a-R744 CRS. That is, in a CRS, R134a can be replaced by R152a. Turgut and Turgut

(2019) investigated CRS's performance with refrigerant pairs R744-R717, R744-R134a, and R744-R1234yf. R744-R1234yf CRS was discovered to have a high efficiency and a low annual cost. Amaris et al. (2019) examined the energy and exergy of a standard R744 booster refrigeration unit, a R744 parallel-compressor booster refrigeration unit, and a R717-R744 CRS. They discovered that the R717-R744 CRS operates better with an ambient temperature of up to 26 °C. Khalilzadeh et al. (2019) presented a novel integrated system powered by solar energy that combines a R744-R717 CRS and an Organic Rankine Cycle. The suggested system was evaluated using energy, exergy, exergoeconomic, and exergoenvironmental assessments. It was discovered that the COP of the integrated system is approximately 5.74 times greater than that of the standard CRS. Sánchez et al. (2019) conducted an experimental comparison of an R134a-R744 CRS and an indirect CRS with R744 as LTR and R152a, R1234ze(E), R290, and R1270 as HTRs. The results showed that the indirect CRS has a 2.5–17.1% rise in energy consumption, a 58.5% reduction in refrigerant mass charge, and a 30% reduction in environmental effect. Adebayo et al. (2021) performed the performance comparison of a CRS with R744 as LTR. It was determined that the refrigerant pair R717-R744 has the highest COP, and HFE7000 is a promising refrigerant that might be used in place of R134a. Unlike prior research, Alkhulaifi and Mokheimer (2022) used water as HTR and R744, R744A, R41, R717, R290, and R1270 as LTRs, and then performed a complete thermodynamic analysis on a CRS. They discovered that the refrigerant pair R717-R718 performs better, with a COP boost of 2.9–8.6%. Furthermore, they stated that there is no risk of freezing when utilizing water in CRS.

R744, in addition to being an LTR, can also be used as HTR in CRS. Colorado et al. (2012) investigated the thermodynamic performance of CRS in HTC with R744 and LTC with R717, R134a, butane R600, and propane R290. They discovered that the COP of R600-R744 CRS is 7.3% higher than that of R717-R744 CRS. Bhattacharyya et al. (2009) investigated the thermodynamics of a CRS with R744A as LTR and R744 as HTR. The effects of various design and operation parameters on CRS's performance were compared. It was demonstrated that adding an internal heat exchanger has no discernible influence on system performance improvement.

In addition to R744, refrigerant R23 and natural refrigerants R41 and R170 are also utilized as LTRs in CRS (Mota-Babiloni et al. 2020). Kilicarslan and Hosoz (2010) investigated the energy performance and irreversibility of a CRS using R23 as LTR. After comprehensive comparisons, refrigerant couples R152a-R23 and R404a-R23 were proposed as replacements for refrigerants R717-R23 and R507-R23. Sarkar et al. (2013) developed a theoretical model to assess the performance of a CRS containing R170, R1150, and R744A in LTC and R717 in HTC. They

discovered that the R717-R170 CRS has the best operation performance, while the R717-R744A CRS has the best volumetric cooling capacity. Sun et al. (2016) compared the performance of an R41-R404A CRS to an R23-R404A CRS using the first and second laws of thermodynamics. The discharge temperature, coefficient of performance (COP), exergy destruction, and exergy efficiency were determined and compared. They suggested that the refrigerant pair R41-R404A could be a preferable substitute for R23-R404A in CRS. Sun et al. (2019) then evaluated the energy and exergy of low GWP refrigerants in CRS using R23, R41, and ethane R170 as LTRs. They came to the conclusion that R41 and R170 are better LTRs. Furthermore, they discovered that the R41-R161 and R41-R717 CRS have better operation performances. Roy and Mandal (2019) compared the operation performance of R41-R404A and R170-R161 CRSs. The R170-R161 CRS has a better ideal COP and exergetic efficiency, according to the researchers. Furthermore, Roy and Mandal (2020) conducted a thorough investigation of a CRS from energetic, exegetic, economic, and environmental perspectives. The refrigerant pair R41-R161 attained the highest exergetic efficiency of CRS by using R41 and R170 as LTRs and R404A and R161 as HTRs. Aktemur et al. (2021) conducted energy and exergy analyses on CRS using refrigerant R41 in LTC and R1243zf, R423A, R601, R601A, R1233zd (E), and RE170 in HTC. The refrigerant pair R41-RE170 was discovered to have the best operation COP and exergy efficiency, and RE170 can be used as an alternate refrigerant for R423A. Aktemur and Ozturk (2021) investigated the performance of a subcritical CRS with an internal heat exchanger. R41 is employed as an LTR, and R601, R602A, and cyclopentane are used as HTRs. Following rigorous evaluations, they discovered that the refrigerant pair R41-R601 has the best thermodynamic performance among three refrigerant pairs. Mouneer et al. (2021) used R170 as LTR and performed thermodynamic analysis on a CRS with R32, R123, R134A, R404A, R407C, R410, and R290 as HTRs to generate -80 °C low temperature. The top three best exegetic efficiencies were discovered to be produced by refrigerant pairs R123-R170, R290-R170, and R134-R170, with values of 40%, 38%, and 35%, respectively. As a result, natural refrigerants R290-R170 are advised for CRS in order to create an ultralow-temperature zone. Udroiu et al. (2022) built a thermodynamic model using R170 as LTR and R290 as HTR to compare the performance of 42 different refrigeration system setups. Rodriguez-Criado et al. (2022) refitted a package R290 refrigeration unit with R170 to achieve ultralow-temperature freezing. The COP of the retrofitted refrigeration unit ranges from 0.6 to 1.6 with evaporation temperatures ranging from -65 °C to -80 °C.

It is clear from the introduction above that R744, R23, R744A, and R170 are frequently chosen as LTC fluids in CRS. Furthermore, less research focuses on CRS at ultralow

temperatures. The natural refrigerant R170 is regarded as a viable LTR employed in CRS to realize ultralow temperatures because of the high operating pressure of R744 and R744A and the high GWP of R23. The little amount of associated experimental research on R170 as LTR in CRS is primarily concentrated on energy and exergy analysis. Despite the fact that Rodriguez-Criado (2022) used R170 in experiments, the evaporation temperature is between -65 °C and -80 °C. There has not yet been an experimental research of CRS at refrigeration temperatures below -86 °C. The low temperature of -80 °C was experimentally measured in a low-temperature freezer by Liu et al. (2023) and Tan et al. (2023) utilizing a cascade refrigeration cycle with refrigerants R170 and R290. Their research demonstrated that it is both feasible and appropriate to produce low temperatures of -80 °C utilizing R290-R170 CRS.

In order to comply with the requirements of the European Union F-Gas Regulation 517/2014, the environmental-friendly refrigerants R170 and R290 are selected to be LTR and HTR in CRS, and are employed in this study to create -86 °C ultralow-temperature. The operation performance of a -86 °C freezer is experimentally examined under two different ambient circumstances with a focus on the storage and transportation of COVID-19 vaccinations. The pull-down and steady operation processes of the -86 °C freezer are both studied. The power usage of CRS is assessed. Some significant conclusions are reached. The current study is important for gaining a thorough understanding of the operation performance of -86 °C CRS freezer and achieving global environmental sustainability.

System description and experimental setup

Experimental schematic diagram

Figure 1 depicts the schematic diagram (Liu et al. 2023, Tan et al. 2023) of the CRS for a -86 °C ultralow-temperature freezer. As can be seen, the CRS is made up of an HTC and an LTC. The HTC consists primarily of a high-temperature compressor, a condenser, a high-temperature capillary, an anti-condensation loop, a drying filter, and a liquid reservoir, whereas the LTC consists of a low-temperature compressor, a precooled condenser, a drying filter, a low-temperature capillary, an evaporator, and an oil separator. The HTC and LTC are connected by a cascade heat exchanger (CHE). Different components are connected in sequence by copper pipe.

In this experiment, a precooled condenser is placed before CHE in LTC. This enhancement could lower the heat exchange burden of the CHE and significantly cool the LTR. As a result, LTC may readily generate extra-low temperatures. Furthermore, an anti-condensation loop is installed

Fig. 1 Schematic diagram of CRS (Tan et al. 2023; Liu et al. 2023)
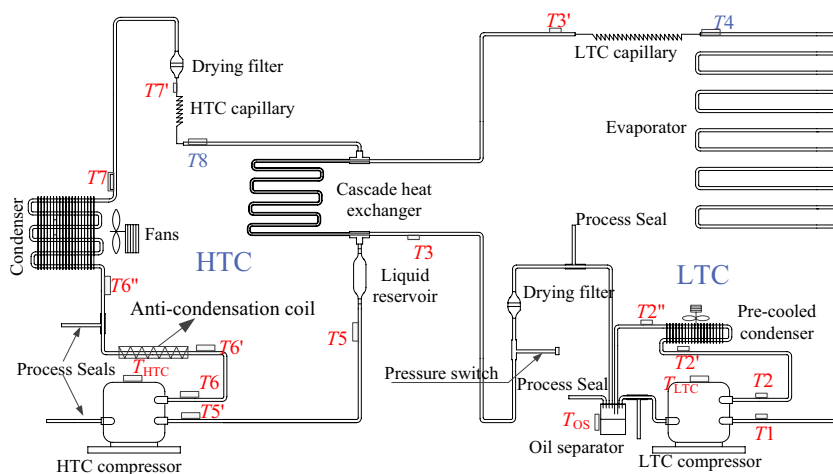
after the HTC compressor and is placed beneath the sealing area of the freezer's exterior door. HTR gas exits the HTC compressor and enters the anti-condensation loop. Condensation of water vapor close to the freezer's external door can be avoided when heated by HTR gas. Meanwhile, the anti-condensation loop can significantly cool the HTR gas, resulting in a noticeable temperature decrease.

Different monitors are configured to gather fluid temperature variations in order to investigate the operation performance of the CRS freezer. Two thermocouples are typically installed at the inlet and outlet of key components. In LTC, monitors $T1$ and $T2$ are installed at the inlet and outlet of low-temperature compressor, monitors $T2'$ and $T2''$ are installed at the inlet and outlet of precooled condenser, and monitor $T3$ and $T3'$ is set at the inlet of CHE and LTC capillary. As for HTC, monitors, installed at the inlet and outlet of the HTC compressor, anti-condensation loop, condenser, capillary, CHE and liquid reservoir, are labelled $T5'$, $T6$, $T6'$, $T6''$, $T7$, $T7'$ and $T5$, respectively. Based on the experimental rig, the related P–h diagram of the CRS is shown in Fig. 2. Hence, the thermal dynamic states of various temperature test points can be easily found from the P–h diagram.

Along with above monitors, three thermocouples labeled T_{LTC}, T_{HTC} and T_{OS} are mounted to the chamber walls of two compressors and an oil separator. Furthermore, because the CHE is a small heat exchanger and the LTC evaporator is encased in foam layer, it is difficult to set monitors to measure fluid temperature at the input of both devices. As a result, $T4$ and $T8$ monitors after capillary are not established in experiments.

Experimental setup

The experimental apparatus of a -86 °C ultralow-temperature freezer and associated test instruments are shown in Fig. 3. The test is performed in a Type-laboratory, where varied dry bulb and wet bulb temperatures can be established. The
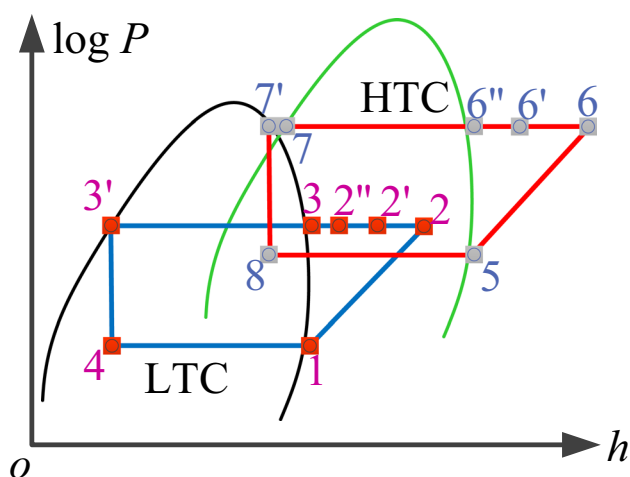

Fig. 2 P–h diagram of CRS

test freezer is made up of an inner box and an outside box, both are composed of iron sheet. The size of the inner box is $588 \times 710 \times 1310$ mm (W×L×H), and the size of the outer box is $873 \times 968 \times 1980$ mm (W×L×H). To decrease heat leakage from external environment, the space between the inner and outer boxes is filled with foam. The foam layer in freezer's top, left, back, and right sides is 90 mm thick, while the foam layer at the bottom of the inner box is 130 mm thick to decrease heat invasion. The inner box contains 552 L of storage space divided into four cabinets. Each cabinet has a capacity of 138 L. As indicated in Fig. 3(a), four interior doors and a separate external door are installed to reduce cold loss from freezer. Internal and external doors have thicknesses of 34 mm and 81 mm, respectively. Apart from LTC evaporator and capillary, the primary components of CRS are located at the bottom of the inner box. This is due to the fact that two compressors, a condenser, a CHE, and other associated components take up too much space and have a
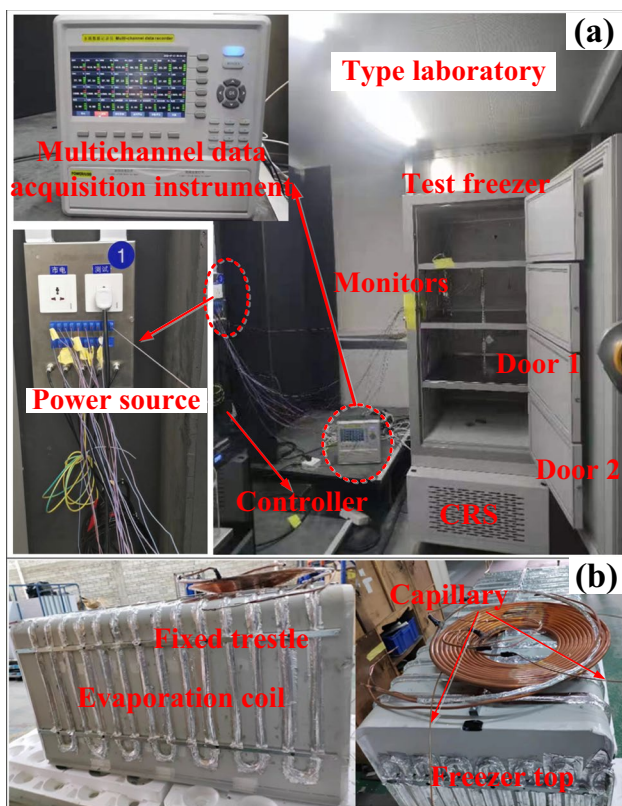
Fig. 3 Experimental rig of low-temperature freezer (**a**) and evaporation coil (**b**)

high mass. Putting these components together and arranging them beneath the inner box can save more refrigeration space while also increasing freezer's operational stability. The HTC evaporator is handcrafted from copper tube and is coiled around the inner box's wall from top to bottom, as shown in Fig. 3(b). The evaporator is linked to low-temperature capillary, which is embedded in foam layer.

Two SC21CNX.2 LBP compressors are adopted. R290 and R170 charge quantities are 155 g and 103 g, respectively. A finned tube heat exchanger is used as condenser. Driven by a fan, external air exchanges heat with HTR gas. HTR gas is eventually condensed to pure liquid after being cooled by external air. In addition, a small finned tube condenser is installed in LTC. Cooled by external air, R170 gas has a noticeable temperature decrease through precooled condenser, which is significant for reducing CHE heat load and achieving a significantly lower evaporation temperature. A casing heat exchanger is chosen as CHE. Table 1 lists the detailed specifications of the CRS's main components (Liu et al. 2023, Tan et al. 2023).

The power source has a voltage of 220 V and a frequency of 50 Hz. The power consumptions of two compressors and fans are measured using a wattmeter. The power meter's measurement accuracy is 0.3%FS. Several test stations are set up to monitor variations in system pressure and temperature to assure the safe operation of the CRS. When overpressure and overheating occur, the emergency cut-off safeguard is activated. Furthermore, several temperature test points are established in freezer to control the start-stop switch of CRS.

The T-type thermocouple is used to measure fluid temperature at the entrance and exit of different components, as well as air temperature in freezer. As seen in Fig. 3, a multichannel data acquisition instrument (Liu et al. 2019, Liu and Tan 2019) is used to collect temperature data from several monitors. The measure uncertainty of the T-type thermocouple is ± 0.5 °C with a temperature range of -150—350 °C. The shallow groove in pipe is formed to improve the test accuracy, and the thermocouple is pasted to groove and coated with dielectric adhesive tapes. As Fig. 1 shows, 13 thermocouples, 6 for LTC and 7 for HTC, are installed in CRS to monitor temperature fluctuations of refrigerants R290 and R170. Furthermore, three

Table 1 Specifications of the main components

Component	Specifications
HTC/LTC compressor	Type: SC21CNX.2 LBP, Displacement: 20.95 cm^3, Max. operation pressure: 2.0 MPa, Max. discharge temperature: 55 °C, Frequency: 50 Hz
Condenser	Type: Finned tube heat exchanger, Diameter of cooper pipe $\Phi 7 \times 0.35$ mm, Thickness of fin: 0.2 mm, Fin spacing: 2 mm, Dimension: $350 \times 130 \times 225$ mm (L×W×H), heat transfer area: 1.78m^2
High-temperature capillary	Processed by copper tube, Diameter: $\Phi 2.7 \times 0.65$ mm, Length: 3.4 m
Cascade heat exchanger	Type: Casing heat exchanger (made by copper pipe), Diameter of outer copper pipe: $\Phi 12.71*0.8$ mm, Diameter of inner copper pipe: $\Phi 6*0.65$ mm, Length: 15.8 m, heat transfer area: 0.29m^2
Low-temperature capillary	Processed by copper tube, Diameter: $\Phi 2.7 \times 0.65$ mm, Length: 5.6 m
Evaporator	Type: Coil heat exchanger (made by copper pipe) with Aluminum fin, diameter of copper pipe: $\Phi 9.52 \times 0.8$ mm, Length: 36 m, heat transfer area: 1.076m^2
Pre-cooled condenser	Type: Finned tube heat exchanger, Diameter of cooper pipe $\Phi 7 \times 0.35$ mm, Thickness of fin: 0.2 mm, Fin spacing: 2 mm, Dimension: $350 \times 130 \times 75$ mm (L×W×H), heat transfer area: 0.41m^2
Oil-separator	Type: Temprite 900
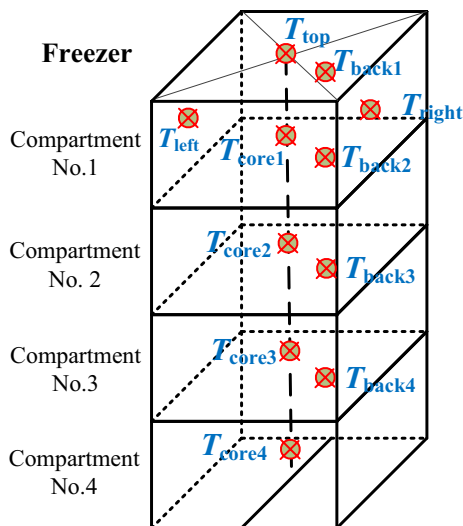
Fig. 4 Temperature test point distribution in freezer

Fig. 5 Variations of dry bulb and wet bulb temperature

temperature monitors are attached to the chamber walls of HTC compressor, LTC compressor, and oil-separator, respectively.

In addition to various state monitors, 11 temperature monitors are set up in freezer to analyze detailed air temperature distribution. As Fig. 4 shows, 4 cabinets are labeled No.1-No.4 from top to bottom. It contains a core temperature monitor and a back temperature monitor for each compartment. A copper bar is used to fix the thermocouple to test the core temperature in each compartment. The back monitor is directly tied to the inner box's wall. T_{core1}-T_{core4} are the compartment numbers for four core monitors, and T_{back1}-T_{back4} are the compartment numbers for four back monitors. In addition, three thermocouples, labeled T_{left}, T_{right} and T_{top}, are attached to the left, right, and top sides of compartment No.1.

Results and discussion

The operation performance of the -86 °C freezer has been tested experimentally. The experiment was conducted in a Type-laboratory at two different dry bulb and wet bulb temperatures. In the Type-laboratory, the relative humidity is set as 65%.

Dry bulb temperature of 25 °C

As Fig. 5 shows, the CRS operates for approximately 1200 min with a dry bulb temperature T_{dry} of 25.0 °C and a wet bulb temperature T_{wet} of 20.2 °C. The associated temperature variations of different monitors are described.

Temperature variation of different state monitors of HTC and LTC

Figure 6 displays the temperature changes of different state monitors in LTC. It is easy to see different monitors all experience initial temperature drops while the CRS is activated. Generally, the pull-down process can be separated into three phases, including early start-up (ESU), rapid temperature drop (RTD) and stable temperature drop (STD) phases. The three phases were also observed in Wang's experiments (Wang et al. 2020). Three phases take 25 min, 95 min, and 412 min, respectively. During the first 25 min, suction temperature $T1$ drops somewhat, whereas discharge temperature $T2$ rises initially and reaches a maximum temperature of 102.8 °C in 25 min. Temperature drops also occur in other monitors, including $T2'$, $T2''$, $T3$ and $T3'$. Distinct monitors have different temperature profiles and temperature changes during ESU period. After 25 min, the freezer enters RTD phase, and different monitors suffer rapid temperature reductions, as illustrated in Fig. 6. This phase lasts 95 min. Temperature drops of monitors $T1$-$T3'$ are 21.4 °C, 12.0 °C, 14.2 °C, 3.2 °C, 2.2 °C and 2.8 °C, respectively, with temperature drop rates of 3.52 °C/hour, 7.58 °C/hour, 8.97 °C/hour, 2.02 °C/hour, 1.39 °C/hour and 1.77 °C/hour. Following that, the CRS enters STD period, which lasts 532 min. Temperatures of different monitors, with the exception of monitor T1, slowly decrease during STD phase. When -86 °C is reached, the final values of monitors $T2$-$T3'$ are 85.3 °C, 53.2 °C, 29.3 °C, 29.2 °C and 27.3 °C, respectively. When it comes to monitor $T1$, its temperature fluctuates dramatically. The primary cause is as follows. The temperature rise of $T1$ is caused by environmental heat leaking through suction pipe between evaporator and LTC compressor. Furthermore, bits of liquid droplets are combined in LTC compressor's suction. The liquid droplet evaporates, lowering the
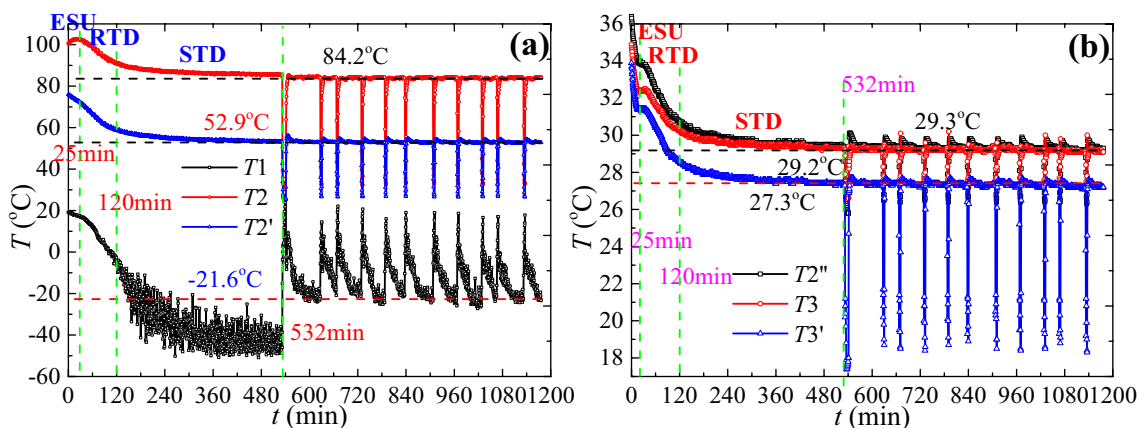
Fig. 6 Temperature distribution of different test points of LTC

refrigerant temperature. As a result, $T1$ experiences noticeable temperature oscillations and drops to -45.9 °C while the CRS ceases.

The CRS enters a periodic start-stop switching phase after 532 min. Based on Fig. 6, it is clear that, aside from monitor $T1$, other monitors all have a tendency to certain temperatures. $T2$ is held at 84.2 °C, the input and outlet gas temperatures of precooled condenser are kept at 52.9 °C and 29.3 °C, respectively, and the inlet temperatures of the CHE and LTC capillaries are 29.2 °C and 27.3 °C, respectively. According to comprehensive investigation, the temperature drop from the output of LTC compressor to the inlet of the precooled condenser is 31.3 °C, whereas the temperature drop via precooled condenser is 23.6 °C. That is to say the long connecting pipe has a greater cooling impact than the precooled condenser. This is mostly due to the fact that the environment temperature is fixed at 25 °C and the discharge temperature of the compressor surpasses 80 °C. The considerable temperature difference leads to the high-temperature discharge gas being greatly cooled. $T2''$ and $T3$ monitors practically have the same temperature with only 0.1 °C difference. It means that the temperature difference between the precooled condenser outlet and the CHE can be ignored. While refrigerant R170 flows through CHE and arrives at the inlet of capillary, its temperature remains almost constant at 27.3 °C.

Figure 7 depicts temperature variations of various HTC monitors. It is apparent that the HTC likewise goes through an initial adjustment. In contrast to LTC, temperature variations in HTC exhibit minor temperature decreases or rises. Aside from HTC compressor discharge gas monitor $T6$, all other monitors show early temperature drops. $T6$ experiences an initial temperature rise and achieves the maximum temperature 106.8 °C in 50 min. The initial pull-down operation takes 120 min. Since then, different monitors remain constant. The HTC achieves stable functioning 412 min earlier
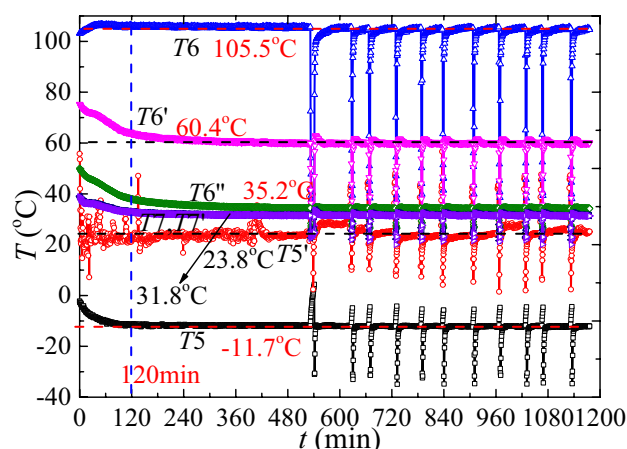

Fig. 7 Temperature distribution of different test points of HTC

than the LTC. Furthermore, it appears that the pull-down process has slight effect on the operation performance of the HTC. The CRS enters periodic start-stop switch 412 min later. Monitor $T5'$ has the most noticeable fluctuation profile. This phenomena also occurs at LTC compressor's inlet for similar reasons. While the HTC is stable, the average temperatures of monitors $T5$-$T7'$ are -11.7 °C, 105.5 °C, 60.4 °C, 35.2 °C, 31.8 °C and 31.7 °C, respectively. $T5'$ changes constantly, but its average temperature is 23.8 °C. When high-temperature R290 gas flows from HTC compressor to anti-condensation loop, it is considerably cooled by cold air from outside, with a temperature drop ($T6$-$T6'$) of 45.1 °C. R290 is chilled in anti-condensation loop by penetration cold capacity from the freezer and external air flow. The temperature drop ($T6'$-$T6''$) through the anti-condensation loop is about 25.2 °C, which is lower than the temperature drop through the long connecting pipe. The pipeline length from HTC compressor to anti-condensation loop can be correctly decreased to improve the temperature

reduction effect created by anti-condensation loop. Following that, HTR gas passes through condenser and toward capillary. It is obvious that a temperature difference of 3.4 °C exists between the condenser's inlet and outlet. The primary causes are stated. (1) There is still a long pipe connecting $T6''$ monitor to HTC condenser. (2) The refrigerant at the condenser's exit may be subcooled. (3) A visible pressure drop occurs when refrigerant runs through HTC condenser. All of the following factors contribute to the difference between $T6''$ and $T7$. Only 0.1 °C temperature difference is generated as the refrigerant fluid travels to LTC capillary. As a result, the temperature of the refrigerant is nearly constant from the condenser outlet to the capillary inlet.

Figure 8 depicts the fluctuations in wall temperature of two compressors and an oil separator. Both HTC compressor and oil separator have obvious wall temperature reductions. The oil separator experiences an early wall temperature drop as a result of CRS startup, while high-temperature compressor experiences a rapid wall temperature rise in the

Fig. 8 Wall temperature variations of two compressors and one oil separator

first 25 min. Following that, both have a quick temperature drop and a slow temperature reduction since 25 min. The wall temperature of low-temperature compressor chamber increases rapidly in the first 120 min, then gradually slows and lasts to 532 min. The CRS enters periodic start-stop switch once -86 °C is reached. The average temperatures of T_{LTC}, T_{HTC} and T_{OS} after 11 operating cycles are 61.6 °C, 40.2 °C and 28.8 °C, respectively. Furthermore, T_{OS} is always lower than T_{LTC}. Generally, lubricant oil has significant cooling effect on low-temperature compressor with a temperature difference of 32.8 °C.

Temperature variation of different monitors in freezer

The temperature changes of different core monitoring and back monitors in freezer are shown in Fig. 9. It is clear that once the CRS is activated, all core monitors suffer a rapid temperature drop. The ESU of CRS appears to have minor influence on the quick temperature reductions of different monitors. Different core monitors enter a consistent temperature drop period since 120 min. That is to say the core monitors only undergo two temperature drop phases. The initial temperatures of T_{core1}-T_{core4} are -50.3 °C, -48.3 °C, -40.5 °C and -35.3 °C, respectively. Furthermore, as shown in Fig. 9(a), it takes 356 min, 248 min, 182 min and 151 min for monitors T_{core1}-T_{core4} to reach the desired temperature of -86 °C. The related temperature reduction rates are 6.02 °C/hour, 9.12 °C/hour, 15.0 °C/hour and 20.14 °C/hour, respectively. It is clear to see that monitor T_{core4} has the highest temperature reduction rate and monitor T_{core1} has the lowest temperature reduction rate. This is mostly due to the fact that monitor T_{core1} is only cooled by evaporator coil, but monitor T_{core4} receives cold capacity from both evaporator coil and cold air sink from freezer's top. Hence, when compared to other monitors, T_{core4} has a faster temperature reduction rate and a lower temperature. 532 min later, the freezer enters a periodic start-stop switch phase, and different monitors
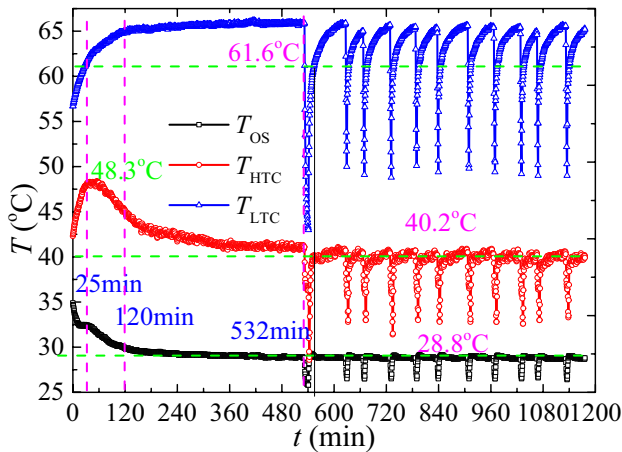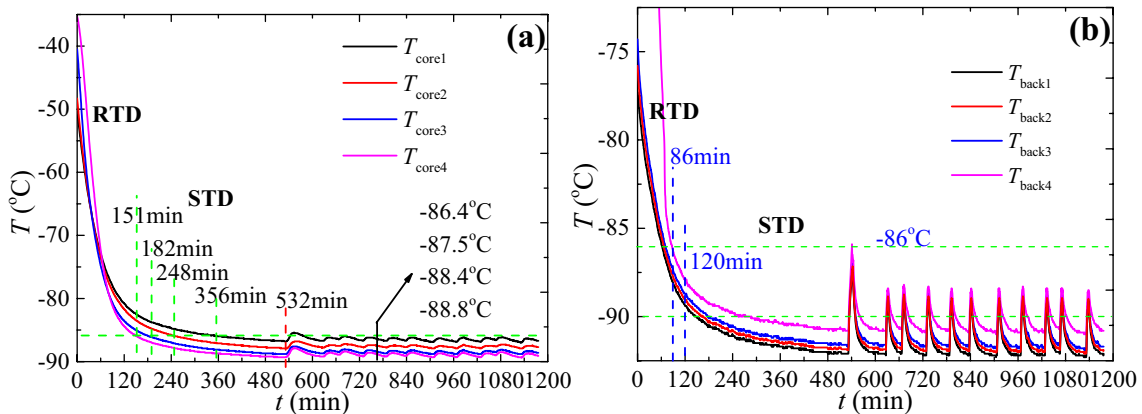

Fig. 9 Temperature variations of different core monitors (**a**) and back monitors (**b**)

show reasonably constant temperature fluctuations. After 640 min start-stop cycle operation, the average temperatures of T_{core1}-T_{core4} are -86.4 °C, 87.5 °C, -88.4 °C and -88.8 °C, respectively. It can be seen that the temperature of the core monitor reduces from top to bottom.

As Fig. 9(b) shows, different back monitors also experience RTD in the first 120 min, and then undergo STD. Different from core monitors, four back monitors dropped to -86 °C in the first 86 min. Due to heat transfer temperature difference and thermal resistance, the air temperature in the freezer is still higher than -86 °C. When the interior temperature of the freezer reaches -86 °C, temperatures of four back monitors are -92.1 °C, -91.9 °C, -91.7 °C and -90.8 °C, respectively. Since then, temperatures of four back monitors enter periodic fluctuation variations. Moreover, it is easy to find the temperature of back monitors rises from top to bottom, which is opposite to the temperature variation trend of core monitors. This is mostly due to the fact that the temperatures of back monitors reflect temperature changes of refrigerant within evaporation coil. While core monitors display air temperature in the freezer, the air temperature is determined by a mix of cooling from evaporation coil and natural convection within the freezer. As a result, the temperature of back monitors steadily falls in the flow direction. Temperatures of various monitors are generally below -86 °C, with the lowest temperature of -92.8 °C.

Power consumption

Figure 10 presents the variation of power consumption P of CRS compressors and fans. When the CRS is turned on, P rises to 1176.1 W. During pull-down process, P drops rapidly for the first 120 min and then undergoes stable decrease. Once the CRS ends in 532 min, the consumed power is about 865.6 W. Thereafter, P experiences cyclical fluctuations and ranges in 865.6–925.5 W. The average power consumption is about 872 W.

Dry bulb temperature of 32 °C

With $T_{dry} = 32$ °C and $T_{wet} = 26.5$ °C, the experimental test on the ultralow-temperature freezer lasts for 1440 min, as shown in Fig. 11. The associated temperature variations of different test points are monitored and introduced.

Temperature variation of different state monitors of HTC and LTC

Figure 12 displays the temperature variations of various monitors in LTC. Here, two operation start-stop cycles are tested with $T_{dry} = 32$ °C and $T_{wet} = 26.5$ °C. Cycle 1 lasts around 960 min and cycle 2 operates for 292 min.
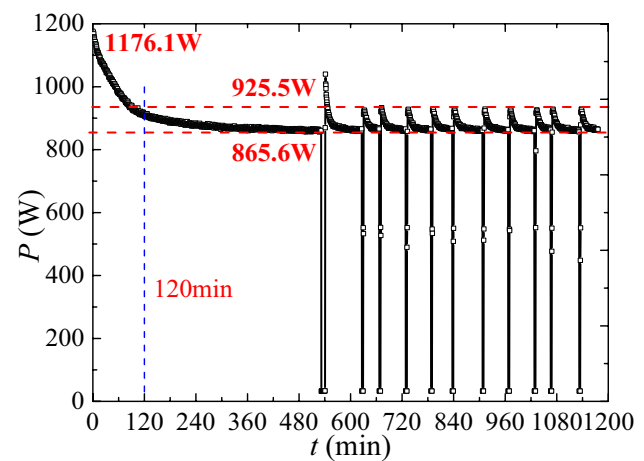

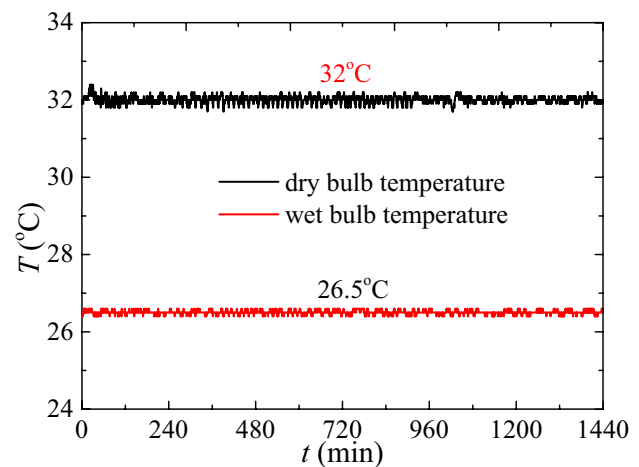**Fig. 10** Power consumption of CRS

Fig. 11 Variations of dry bulb temperature and wet bulb temperature

As Fig. 12 shows, the CRS enters stable operation after 10 min of adjustment. Aside from suction gas temperature $T1$, other monitors all have stable operation temperature values. For example, the discharging vapor temperature $T2$ of LTC compressor is typically 94.1 °C, while the inlet temperature $T2'$ and outlet temperature $T2''$ of precooled condenser are kept to 63.2 °C and 37.1 °C, respectively. The inlet gas temperature $T3$ of CHE after passing through drying filter, is approximately 36.8 °C with a temperature reduction of 0.3 °C, as shown in Fig. 12(b). Flowing through a long connecting pipe, refrigerant temperature $T3'$ before low-temperature capillary is kept to 35.0 °C. It signifies that a temperature difference of 1.8 °C exists between the CHE exit and the inlet of LTC capillary. As for the suction temperature of LTC compressor, $T1$ exhibits significant temperature fluctuations, shown as Fig. 12(a). Generally, $T1$ nearly increases from -54.2 °C to -44.6 °C with noticeable temperature fluctuation
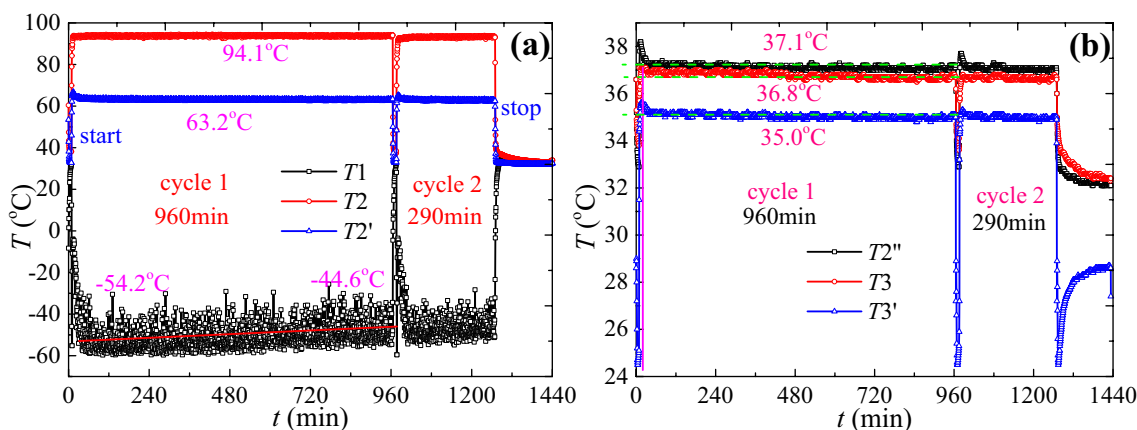
Fig. 12 Temperature distribution of different test points of LTC
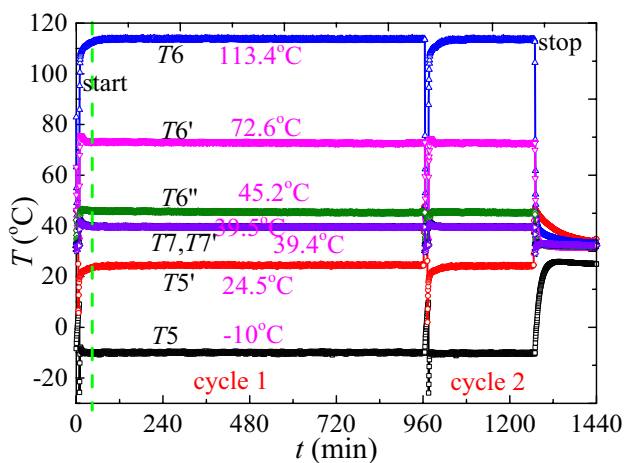

Fig. 13 Temperature distribution of different test points of HTC

during cycle 1. When it comes to cycle 2, monitor $T1$ has a minor temperature reduction, while other monitors remain at the same temperatures.

Figure 13 depicts the temperature variations of various HTC monitors. It is easy to see the CRS comes into stable functioning after a short-term adjustment, and different monitors incline to certain temperature values. The inlet temperature $T5$ and outlet gas temperature $T6$ of HTC compressor remain constant at -10 °C and 113.4 °C, respectively. HTR gas goes through a long connection pipe to anti-condensation loop, and the inlet temperature $T6'$ of anti-condensation loop is around 72.6 °C. It is easy to locate 40.8 °C temperature decrease forms. This is primarily due to the discharge gas temperature being higher than 110 °C and the ambient temperature being set at 32 °C. Because of large temperature difference, the high-temperature discharge gas is cooled by externally chilled air. The outlet gas temperature $T6''$ is approximately 45.2 °C when R170 gas flows through

the anti-condensation. That means the temperature drops by only 27.4 °C. The anti-condensation loop's temperature drop is primarily cooled by cold air from the freezer. Following that, a high-temperature refrigerant gas runs through the condenser with an exit temperature $T7$ of 39.5 °C. It is seen that 4.7 °C temperature difference forms between the inlet and outlet of the condenser. A similar explanation was given above. A temperature difference of 0.1 °C is generated by refrigerant fluid flowing from the CHE exit to the LTC capillary.

Figure 14 depicts the temperature variations on the wall of two compressors and an oil separator. When the CRS is activated, the wall temperature T_{LTC} of LTC compressor rises from 49.4 °C to 71.3 °C and stays there, whereas T_{HTC} rises from 35.0 °C and goes to 47.2 °C during stable operation. The chamber wall of oil separator has low temperature, and T_{OS} rises from 32.6 °C to 36.2 °C. Throughout whole procedure, T_{OS} is lower than T_{LTC}, with an average temperature difference of 35.1 °C. The excellent cooling effect of lubricating oil has been confirmed once more. In cycle 2, three monitors also undergo a fast temperature increase and tend to be constant.

Temperature variation of different monitors in freezer

Figure 15 displays the temperature distributions of air in freezer. Monitors in freezer also have stable temperature changes, which are influenced by stable temperature distribution of different state monitors depicted in Figs. 12–13. As indicated in Fig. 15(a), when the freezer is turned on, four core monitors exhibit initial modest amplitude temperature rises, then slightly decrease and tend to be steady after 180 min. Temperatures of four core monitors tend to stabilize after roughly 180 min. Similar temperature variations also occur in cycle 2. During stable operation, the average temperatures of T_{core1}-T_{core4} finally maintain at
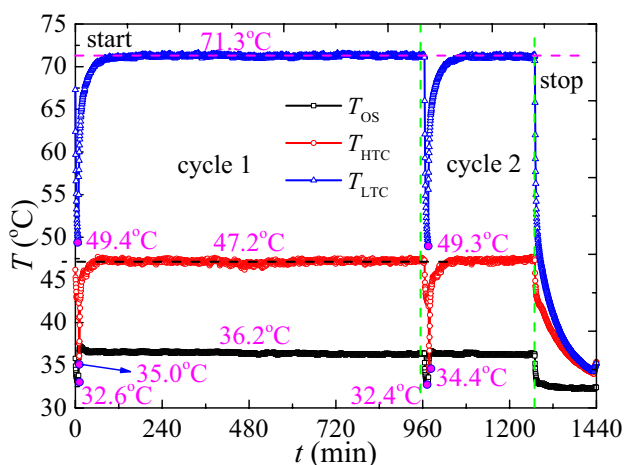
Fig. 14 Temperature variations of two compressors and an oil separator

and are lower than that of core monitors. Furthermore, based on the temperatures of four rear monitors, it is possible to determine that the evaporation temperature of LTC must be less than -90 °C.

Power consumption

The change in P of CRS with $T_{dry} = 32$ °C and $T_{wet} = 26.5$ °C is shown in Fig. 16. It is obvious that when the CRS is activated, P increases rapidly at first and reaches 1137 W. Following then, the CRS experiences short-term adjustment, and P tends to be 935 W during stable operation. P climbs to 1048 W in cycle 2 before remaining constant at 935 W.
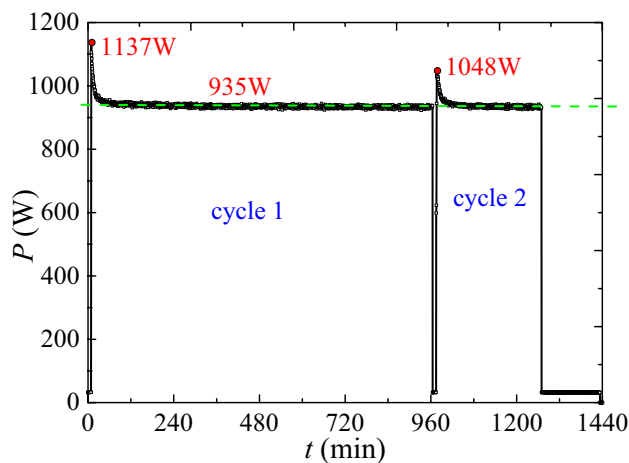
-84.6 °C, -86.1 °C, -87.1 °C and -87.4 °C, respectively. The temperature of the air in the freezer drops from top to bottom. Furthermore, save from some core space in compartment No.1, temperatures in the rest of the freezer all drop to or below -86.0 °C. To realize the entire space of the freezer being cooled down -86.0 °C, some optimism measurements and winding adjustments on the evaporation coil should be performed, such as decreasing the coil interval of the evaporator in compartment No.1 or raising the mass flow rate of refrigerants.

The temperature distributions of four monitors placed at the back of the freezer are shown in Fig. 15(b). Four back monitors exhibit abrupt temperature increases at first, then decrease and stabilize. The final temperature values of monitors T_{back1}-T_{back4} after 180 min adjustment are -90.2 °C, -90.1 °C, -89.9 °C and -89.2 °C, respectively. The temperatures of back monitors rise from top to bottom

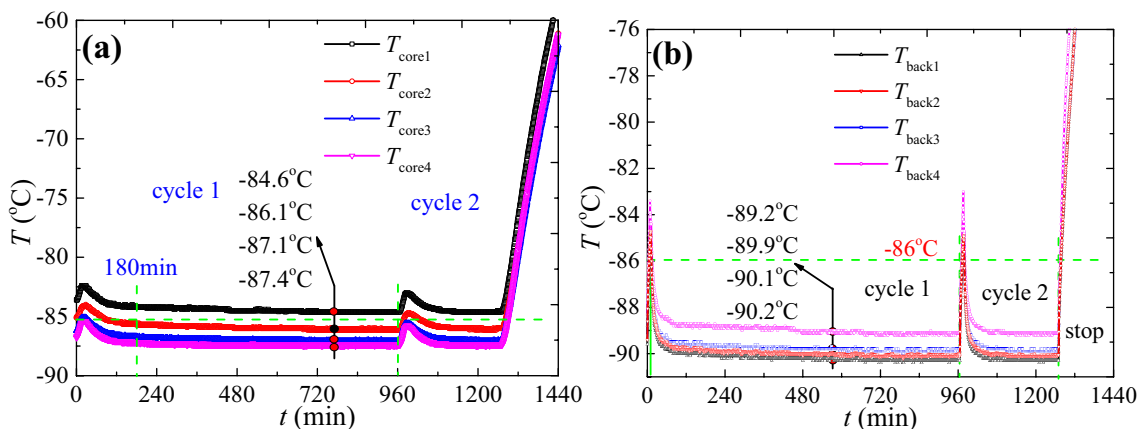**Fig. 16** Power consumption of CRS

Fig. 15 Temperature variations of different core monitors (**a**) and back monitors (**b**)

Discussion and analysis

Based on preceding testing results, the impact of dry bulb and wet bulb temperatures on the operation performance of -86 °C ultra-low-temperature freezer is analyzed. The stable operating temperatures of various state monitors are recorded and compared, with the average temperature of monitor $T1$ being adopted due to its decrease during operation cycle 1. Table 2 displays the stable operating temperatures of various state monitors in the freezer, revealing that $T1$ drops from -21.6 °C to -49.4 °C as T_{dry} increases from 25 °C to 32 °C and T_{wet} increases from 20.2 °C to 26.5 °C. However, the temperatures of other monitors increase alongside $T1$ with T_{dry}/T_{wet} rising from 25/20.2 °C to 32/26.5 °C, resulting in temperature differences between two cases varying from 7.7–10.3 °C. As the ambient temperature increases, more energy is required to pull down to the desired temperature, leading to a noticeable rise in power consumption. The pressure ratio also increases as the temperatures of other monitors rise. The temperature drop through the long connecting pipe between the freezer compressor and precooled condenser is also calculated, with temperature drops in both cases being nearly identical, differing by only 0.4 °C. Additionally, the precooled condenser has a better cooling effect with a temperature drop of 26.1 °C when $T_{dry} = 32$ °C and $T_{wet} = 26.5$ °C, whereas the connecting pipe has a slightly better effect with $T_{dry} = 25$ °C and $T_{wet} = 20.2$ °C. Overall, the length of the connecting pipe can be increased appropriately to reduce the size of the precooled condenser.

Table 3 presents the stable temperatures of different monitors in HTC. In contrast to LTC, the temperatures of different monitors in HTC increase with T_{dry} and T_{wet}. The suction temperature and discharge temperature exhibit temperature changes of 1.7 °C and 6.8 °C, respectively. In this case, the temperature drops through the long pipe connecting the outlet of HTC compressor and the inlet of anti-condensation loop, and through anti-condensation loop, are compared. It is apparent that a higher temperature decline of 46.1 °C occurs through the loop pipe with $T_{dry} = 25$ °C and $T_{wet} = 20.2$ °C, while a 27.4 °C temperature drop is observed in the anti-condensation loop with $T_{dry} = 32$ °C and $T_{wet} = 26.5$ °C. The temperature drop through the long pipe is larger than that in the anti-condensation loop. Properly reducing the length of the connecting pipe can enhance the anti-condensation effect.

To evaluate the cooling performance of the CRS in two different environmental conditions, Table 4 displays the stable air temperatures inside the freezer, as well as the lowest temperatures recorded by four back monitors. In both scenarios, the temperatures of four core monitors decrease from top to bottom. When T_{dry} is set as 25 °C and T_{wet} is 20.2 °C, the entire freezer is chilled to -86.0 °C, and the lowest temperature of the four back monitors reaches -92.8 °C. However, when T_{dry} increases to 32 °C and T_{wet} to 26.5 °C, cabinet No.1 cannot be cooled down to -86.0 °C, while the rest of the freezer reaches the desired temperature. The lowest temperature of the back monitor is -90.2 °C. The heat transfer temperature differences between the evaporator coil and the inner space of the freezer are approximately 6.8 °C and 4.2 °C.

Based on test results, it is found that the power consumption of the -86 °C ultralow-temperature freezer during stable operation increases from 872 to 935 W when T_{dry} increases from 25 °C to 32 °C and T_{wet} increases from 20.2 °C to 26.5 °C. The rise in power consumption is primarily due to the drop in LTC suction temperature and the increase in the discharge temperatures of both LTC and HTC. This results

Table 2 Temperature comparison of different state monitors of LTC

T_{dry}/T_{wet}(°C)	$T1$(°C)	$T2$(°C)	$T2$'(°C)	$T2$''(°C)	$T3$(°C)	$T3$'(°C)	$(T2-T2')$(°C)	$(T2'-T2'')$(°C)
25/20.2	-21.6	84.2	52.9	29.3	29.2	27.3	31.3	23.6
32/26.5	-49.4	94.1	63.2	37.1	36.8	35.0	30.9	26.1

Table 3 Temperature comparison of different state monitors of HTC

T_{dry}/T_{wet}(°C)	$T5$ (°C)	$T5$' (°C)	$T6$(°C)	$T6$' (°C)	$T6$'' (°C)	$T7$ (°C)	$(T6-T6')$(°C)	$(T6'-T6'')$(°C)
25/20.2	-11.7	23.8	106.5	60.4	35.2	31.8	46.1	25.2
32/26.5	-10.0	24.5	113.4	72.6	45.2	39.5	40.8	27.4

Table 4 Temperature comparison of different monitors in the freezer

T_{dry}/T_{wet}(°C)	T_{core1}(°C)	T_{core2}(°C)	T_{core3}(°C)	T_{core4}(°C)	Lowest temperature (°C)
25/20.2	-86.4	-87.5	-88.4	-88.8	-92.8
32/26.5	-84.6	-86.1	-87.1	-87.4	-90.2

in a higher temperature difference between the inlet and exit of two compressors, causing the increase of the pressure ratio and, in turn, leading to higher power consumption. In addition, high dry bulb and wet bulb temperatures cause the increase of heat load in condensers, which increases fan power consumption.

Conclusions

An experimental study was carried out to investigate the operation performance of a -86 °C ultralow-temperature freezer using natural refrigerants R290-R170 under two dry bulb and wet bulb temperatures. Various state monitors and temperature monitors were set up to examine the temperature changes of R290 and R170, and the temperature distribution in freezer during the pull-down and stable operation stages. Some of the most important discoveries are summarized.

Generally, the temperature fluctuations of different state monitors in LTC can be separated into three stages during the pull-down operation, namely EST, RTD, and STD. With $T_{dry} = 25$ °C and $T_{wet} = 20.2$ °C, the EST phase lasts 25 min, during which different monitors undergo initial temperature adjustments. During the RTD phase (25–120 min), different monitors experience rapid and significant temperature reductions. The longest of the three stages is the STD phase, where various monitors experience small temperature drops. The HTC has no discernible influence on temperature fluctuations across different monitors. The core and back monitors undergo rapid temperature drops before entering the STD phase. The temperature drop rates of the inlet and outlet of LTC compressor are 13.52 °C/hour and 7.58 °C/hour, respectively. Temperature decrease rates of four core monitors are 6.02 °C/hour, 9.12 °C/hour, 15.0 °C/hour, and 20.14 °C/hour, respectively. While T_{dry} is set as 32 °C and T_{wet} as 26.5 °C, the CRS freezer experiences 10 min adjustment initially and then comes into stable operation, so the initial effect is not introduced here.

Once -86 °C is achieved, the CRS operates periodically and different monitors tend to be steady. Temperature rises are observed across all monitors with T_{dry} ranging from 25 °C to 32 °C and T_{wet} ranging from 20.2 °C to 26.5 °C, except for the suction temperature $T1$ of LTC compressor, which decreases as T_{dry} and T_{wet} increase. As a result, the power consumption has increased by 7.2%. The length of the LTC and HTC connecting pipelines should be adjusted suitably to improve the effects of the precooled condenser and anti-condensation loop. The wall temperature of the oil separator is always lower than that of the LTC compressor, confirming the cooling impact of the lubricating oil on LTC compressor.

The entire freezer space can be cooled to -86 °C with $T_{dry} = 25$ °C and $T_{wet} = 20.2$ °C. When T_{dry} rises to 32 °C and T_{wet} rises to 26.5 °C, some space in cabinet No.1 remains uncooled at -84.6 °C, but the air temperature in cabinets No.2–4 has dropped to -86 °C. Back monitors have the lowest temperatures of -92.8 °C and -90.2 °C in two occasions. This indicates that the current ultralow-temperature freezer can meet the demand for COVID-19 vaccine storage at an environmental temperature of 25 °C. However, improvements should be made to reduce the air temperature in the top cabinet of the freezer when T_{dry} reaches 32 °C.

Declarations

References

Adebayo V, Abid M, Adedeji M (2021) Comparative thermodynamic performance analysis of a cascade refrigeration system with new refrigerants paired with CO2. Appl Therm Eng 184:116286

Aktemur C, Ozturk IT (2021) Energy and Exergy Analysis of a Subcritical Cascade Refrigeration System with Internal Heat Exchangers Using Environmentally Friendly Refrigerants. J Energy Res Technol 143(10):102103

Aktemur C, Ozturk IT, Cimsit C (2021) Comparative energy and exergy analysis of a subcritical cascade refrigeration system using low global warming potential refrigerants. Appl Therm Eng 184:116254

Alkhulaifi YM, Mokheimer E (2022) Thermodynamic Assessment of Using Water as a Refrigerant in Cascade Refrigeration Systems With Other Environmentally Friendly Refrigerants. J Energy Res Technol 144(2):022101

Amaris C, Tsamos KM, Tassou SA (2019) Analysis of an R744 typical booster configuration, an R744 parallel-compressor booster configuration and an R717/R744 cascade refrigeration system for retail food applications. Part 1: Thermodynamic analysis. Energy Procedia 161:259–267

ASHRAE (2014) ASHRAE handbook-refrigeration, SI. ASHRAE, Atlanta, Georgia, US

Bhattacharyya S, Garai A, Sarkar J (2009) Thermodynamic analysis and optimization of a novel N2O–CO2 cascade system for refrigeration and heating. Int J Refrig 32(5):1077–1084

Bingming W, Huagen W, Jianfeng L (2009) Experimental investigation on the performance of NH3/CO2 cascade refrigeration system with twin-screw compressor. Int J Refrig 32(6):1358–1365

Cabello R, Sánchez D, Llopis R (2017) Energy evaluation of R152a as drop in replacement for R134a in cascade refrigeration plants. Appl Therm Eng 110:972–984

Colorado D, Hernández JA, Rivera W (2012) Comparative study of a cascade cycle for simultaneous refrigeration and heating operating with ammonia, R134a, butane, propane, and CO2 as working fluids. Int J Sustain Energ 31(6):365–381

Dopazo JA, Fernández-Seara J (2011) Experimental evaluation of a cascade refrigeration system prototype with CO2 and NH3 for freezing process applications. Int J Refrig 34(1):257–267

Eini S, Shahhosseini H, Delgarm N (2016) Multi-objective optimization of a cascade refrigeration system: Exergetic, economic, environmental, and inherent safety analysis. Appl Therm Eng 107:804–817

Getu HM, Bansal PK (2008) Thermodynamic analysis of an R744–R717 cascade refrigeration system. Int J Refrig 31(1):45–54

Khalilzadeh S, Nezhad AH, Sarhaddi F (2019) Reducing the power consumption of cascade refrigeration cycle by a new integrated system using solar energy. Energy Convers Manag 200:112083

Kilicarslan A, Hosoz M (2010) Energy and irreversibility analysis of a cascade refrigeration system for various refrigerant couples. Energy Convers Manag 51(12):2947–2954

Lee TS, Liu CH, Chen TW (2006) Thermodynamic analysis of optimal condensing temperature of cascade-condenser in CO2/NH3 cascade refrigeration systems. Int J Refrig 29(7):1100–1108

Liu Z, Tan H (2019) Thermal performance of ice-making machine with a multi-channel evaporator. Int J Green Energy 16(7):520–529

Liu Z, Yan J, Gao P (2019) Experimental study on temperature distribution in an ice-making machine multichannel evaporator. Sci Technol Built Environ 25(1):69–82

Liu Z, Bai M, Tan H (2023) Experimental test on the performance of a −80°C cascade refrigeration unit using refrigerants R290–R170 for COVID-19 vaccines storage. J Build Eng 63:105537

Llopis R, Sánchez D, Sanz-Kock C (2015) Energy and environmental comparison of two-stage solutions for commercial refrigeration at low temperature: Fluids and systems. Appl Energy 138:133–142

Mateu-Royo C, Arpagaus C, Mota-Babiloni A (2021) Advanced high temperature heat pump configurations using low GWP refrigerants for industrial waste heat recovery: A comprehensive study. Energy Convers Manag 229:113752

Mota-Babiloni A, Joybari MM, Navarro-Esbrí J (2020) Ultralow-temperature refrigeration systems: Configurations and refrigerants to reduce the environmental impact. Int J Refrig 111:147–158

Mouneer TA, Elshaer AM, Aly MH (2021) Novel Cascade Refrigeration Cycle for Cold Supply Chain of COVID-19 Vaccines at Ultra-Low Temperature-80° C Using Ethane (R170) Based Hydrocarbon Pair. World J Eng Technol 9(2):309–336

Mumanachit P, Reindl DT, Nellis GF (2012) Comparative analysis of low temperature industrial refrigeration systems. Int J Refrig 35(4):1208–1221

Pan M, Zhao H, Liang D (2020) A review of the cascade refrigeration system. Energies 13(9):2254

Rodriguez-Criado JC, Expósito-Carrillo JA, Pérez BP (2022) Experimental performance analysis of a packaged R290 refrigeration unit retrofitted with R170 for ultra-low temperature freezing. Int J Refrig 134:105–114

Roy R, Mandal BK (2019) Energetic and exergetic performance comparison of cascade refrigeration system using R170–R161 and R41–R404A as refrigerant pairs. Heat Mass Transf 55(3):723–731

Roy R, Mandal BK (2020) Thermo-economic analysis and multi-objective optimization of vapour cascade refrigeration system using different refrigerant combinations. J Therm Anal Calorim 139(5):3247–3261

Sánchez D, Cabello R, Llopis R (2019) Energy assessment and environmental impact analysis of an R134a/R744 cascade refrigeration plant upgraded with the low-GWP refrigerants R152a, R1234ze (E), propane (R290) and propylene (R1270). Int J Refrig 104:321–334

Sarkar J, Bhattacharyya S, Lal A (2013) Performance comparison of natural refrigerants based cascade systems for ultra-low-temperature applications. Int J Sustain Energ 32(5):406–420

Sun Z, Liang Y, Liu S (2016) Comparative analysis of thermodynamic performance of a cascade refrigeration system for refrigerant couples R41/R404A and R23/R404A. Appl Energy 184:19–25

Sun Z, Wang Q, Xie Z (2019) Energy and exergy analysis of low GWP refrigerants in cascade refrigeration system. Energy 170:1170–1180

Tan H, Xu L, Yang L (2023) Operation performance of an ultralow-temperature cascade refrigeration freezer with environmentally friendly refrigerants R290–R170. Environ Sci Pollut Res 30:29790–29806

Turgut MS, Turgut OE (2019) Comparative investigation and multi objective design optimization of R744/R717, R744/R134a and R744/R1234yf cascade refrigeration systems. Heat Mass Transf 55(2):445–465

Udroiu CM, Mota-Babiloni A, Navarro-Esbrí J (2022) Advanced two-stage cascade configurations for energy-efficient–80° C refrigeration. Energy Convers Manag 267:115907

Wang H, Song Y, Cao F (2020) Experimental investigation on the pull-down performance of a-80° C ultra-low temperature freezer. Int J Refrig 119:1–10